Full Paper

Wiley Online Library

ELECTROANALYSIS

DOI: 10.1002/elan.202060378

Experimental and Theoretical Studies on the Protective Effect of a Biomass Corrosion Inhibitor (*vigna radiata*) on Mild Steel in Acidic Medium

Chidiebere A. Maduabuchi,*[a, g] Demian I. Njoku,*[b, g] Obike I. Anthony,[c] Simeon C. Nwanonenyi,[d, g] Christogonus Akalezi,[e, g] Adindu Blessing,[f] and Emeka E. Oguzie[g]

Abstract: The scrutiny of the impeding properties of *vigna radiata* (VR) on mild steel corrosion in sour environs (1 M HCl and 0.5 M H_2SO_4) was done by means of gravimetric, electrochemical impedance spectroscopy (EIS) and potentiodynamic polarization methods (PDP). Polarization findings revealed that VR retarded the corrosion process in a mixed-mode manner. Adsorption of the active components of VR was found to be in line with Langmuir adsorption isotherm. The obtained PDP result was complemented by the EIS findings. Scanning electron microscopy (SEM), atomic force microscopy (AFM) and the theoretical technique was used to complement the results.

Keywords: Acid corrosion · AFM · EIS · Mild steel · Polarization · DFT · Adsorption Energy

1 Introduction

Different techniques could be employed in a quest to retard the corrosion rate, however, the use of non-poisonous corrosion inhibitors is a good procedure and biomass corrosion inhibitors (BCI) are beneficial in this regard [1]. These non-poisonous corrosion inhibitors when inoculated in infinitesimal quantities to the aggressive environments have the potential to block the corrosion of metals and their alloys.

In literature, numerous organic compounds have been recognized to be good and effective corrosion inhibitors; they have heteroatoms (nitrogen, oxygen, sulfur, phosphorus) and manifold bonds/aromatic rings in their arrangements [1–4]. The key points that define the level of inhibition efficiency (IE) in these functional groups consist of the presence of lone pairs of electron and slackly bound pi-electrons [5–7]. The resultant modification in the mechanism of the corrosion process is ascribed to the interaction of these organic inhibitors with the corroding steel surface which is via adsorption. Studies have revealed some significant factors that are responsible for the adsorption strength of these inhibitors; they are, but not limited to chemical and structural features of the adsorbed layers. They are usually formed at a specific state [8]. Apart from all these, most of the organic inhibitors are poisonous for human beings and the environment at large, joined with the fact that they are costly.

In our current world, improved ecological sensitization and strict environmental regulations, has become paramount. So, researchers have now resorted on the use of BCI's to supplant the poisonous brands. In this regard, more than a few studies have been recounted on the use of BCI's in various corrosive environments [9–14], and the obtained results show that BCI's contain several compounds that satiate the needed features. Quite a lot of studies on the use of plant extracts as a corrosion inhibitor for mild steel in acid solutions have been studied [15–25].

The V*R* employed in this work is a legume cultivated for its palatable seeds. It is an annual plant, reaching a height of 0.16 m–1.24 m. It is slightly hairy with a well-

[a] C. A. Maduabuchi
Department of Science Laboratory Technology, Federal University of Technology, Owerri, PMB 1526, Owerri, Nigeria
Phone Number: +2348035162613
E-mail: arinzechukwuchidiebere@gmail.com
Chidiebere.arinzechukwu@futo.edu.ng
[b] D. I. Njoku
Laboratory for Corrosion and Protection, Institute of Metal Research, Chinese Academy of Sciences, 62 Wencui Road, Shenyang, Liaoning, 110016, China
E-mail: demianifeanyi@gmail.com
demian@imr.ac.cn
[c] O. I. Anthony
Department of Chemistry, Abia State University, Uturu, Abia State
[d] S. C. Nwanonenyi
Department of Polymer Science, Federal University of Technology, Owerri, Nigeria
[e] C. Akalezi
Department of Chemistry, Federal University of Technology, Owerri, Nigeria
[f] A. Blessing
Department of Chemistry, Imo State University, Owerri, Nigeria
[g] C. A. Maduabuchi, D. I. Njoku, S. C. Nwanonenyi, C. Akalezi, E. E. Oguzie
Africa Centre of Excellence in Future Energies and Electrochemical Systems, Federal University of Technology, Owerri, Nigeria

developed root system [26]. It is good for the health of eyes, hair, nails and also enhances the blood circulation. This VR is loaded with high amount of fiber and low in calories. It is employed in therapeutic uses such as to detoxify the body and eliminate heat. A GC-MS characterization study has shown that its major components are: caffeine, 5-Hydroxy methylfurfural, linoleic acid and 3-O-Methyl-d-glucose [27]. The structures are presented in Figure 1 below.

The adsorption of an organic inhibitor as stated earlier can be influenced by its chemical structure. To back up this claim, a reasonable number of investigations have reported a relationship between the frontier orbital properties of organic molecules (e.g the energies of the highest occupied molecular orbital (HOMO) and lowest unoccupied molecular orbital (LUMO) and band gap energies (E_{LUMO}–E_{HOMO}), calculated by different quantum mechanical (QM) techniques and corrosion inhibition. For instance, the relationships between corrosion rates with E_{HOMO}, the energy gap, global softness (σ) and hardness (η) for some organic compounds have been described [28,20].

Notwithstanding, these important parameters outlined, it will be good to carefully monitor the interaction between the active sites on these inhibitors and the steel surface. To define this, molecular dynamics simulations (MDS) have been employed to expansively inspect firm adsorption of these active components of VR on the steel surface [3,9]. Employing MDS technique, the adsorption mode of the VR molecules onto the mild steel surface can be determined even at the molecular level. Furthermore, the calculation of the value of the adsorption energy between the organic inhibitor and the steel surface can be determined, with this useful information, the difference in the inhibiting efficacy between different organic inhibitors can be calculated [15].

The current study further investigates the efficacy of VR as a promising environmentally friendly corrosion inhibitor and to further model the electronic and adsorption structures of the selected active components of VR extract using density functional theory (DFT) based quantum chemical computation. Surface probe studies (SEM and AFM was employed to complement the experimental investigations).

2 Experimental

2.1 Preparation of the Working Electrode/Test Solutions

The chemical composition (wt %) of mild steel employed in this work is outlined as follows: C–0.05; Mn–0.6; P–0.36; Si–0.3 and the balance Fe. The sample was progressively polished under running water-using silicon carbide abrasive paper (grade 400 to 1000). After which the samples were washed several times with distilled water dried in acetone and warm air and preserved in desiccators. The test solutions are 0.5 M H_2SO_4 and 1 M HCl. Standard solutions of the VR extract employed in this work were prepared by placing under reflux weighed amounts of the dried and ground leaf of VR in ethanol for duration of 3 hrs. The acquired solutions were allowed to cool and then filtered properly with the aid of a filter

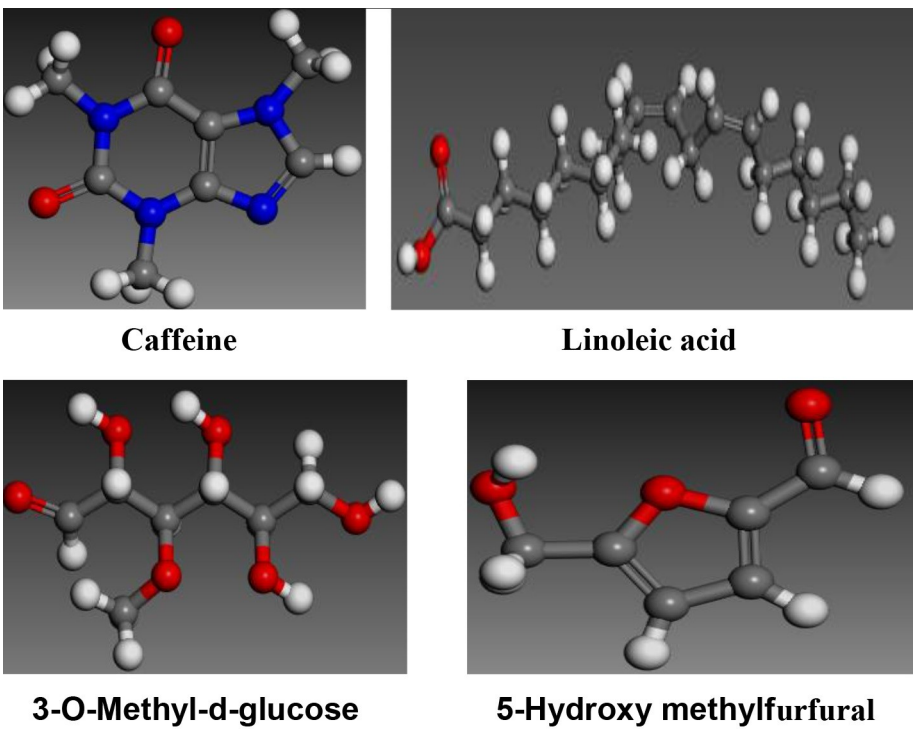

Fig. 1. Structures of some selected constituents of VR extract.

cloth. The quantity of VR material extracted into solution was then quantified by comparing the weight of the dried residue with the original weight of the dried plant material before extraction. Solutions containing the inhibitor were prepared in the preferred concentration range (200 mg/L–1000 mg/L) by diluting the stock extract with the acid solution [12].

2.2 Measurements of Weight Loss

The gravimetric studies were carried out on mild steel samples having dimensions of 30 mm × 30 mm × 1.4 mm. The test samples were cleaned very well, dried and weighed. The weighed samples were then dipped in clean glass 400 ml capacity beakers containing the test solutions with the aid of glass hooks and rods. Studies were thereafter carried out under total dipping conditions in aerated and unperturbed solutions at a temperature of 303 K. The determination of the loss in weight with respect to time, involves withdrawal of the samples at 24-hr intervals for a total period of 120 h. The samples were cleansed with a bristle brush, thoroughly washed, dried, and re-weighed. The difference between the weight of the samples at a specified time and its original weight is regarded as the weight loss. Tests were run twice to certify reproducibility [9].

2.3 Electrochemical Tests

The electrochemical tests (EIS and PDP measurements) were done on the Princeton PAR-2273 Electrochemical System workstation, by means of a three-electrode cell. Graphite rod and a saturated calomel electrode (SCE) served as a counter and reference electrodes. A steel sample that was static in epoxy gum with a surface area of 1 cm^2 exposed to the test solution under investigation was the working electrode. Electrochemical investigations were done in aerated and stagnant environs at the end of 30 minutes of dipping at a temperature of 303 K to get steady state potential. EIS studies were then performed at corrosion potentials (E_{corr}) over a frequency range of 100 kHz–0.1 Hz (29), signal amplitude perturbation of 5 mV was used. Potentiodynamic polarization tests were done by sweeping at a potential range of −250 mV to +250 mV versus corrosion potential at steady state OCP at constant scan rate of 0.5 mV/s [21].

2.4 Surface Probe Analysis

The investigation was complemented by surface morphology scrutiny with SEM and AFM techniques. SEM investigation was performed with the aid of XL-30FEG type scanning electron microscope, while the AFM analysis was done by Picoplus 2500 surface probe microscope.

3D atomic force microscopy studies were carried out using mild steel specimens having dimensions of 15 × 15 × 2 mm, these were dipped in the tests solutions for a period of 24 h in the absence and presence of best concentration of 1000 mg/L VR at 303 K. in each case (for SEM and AFM), the samples for both examinations were removed and cleaned severally with distilled water, dried in warm air and all studies were done in dry conditions, without immersion in the test solution.

3 Computational Details

Density functional theory (DFT) calculations were achieved in the framework of the electronic structure program DMol3, adopting a Mulliken population analysis. Electronic parameters for this important simulation include the Perdew-Wang (PW) local correlation density functional and restricted spin polarization employing DND basis set. The core electrons valuation was achieved at the lowest atomic orbitals, the DFT semicore pseudopotentials (DSPP) was set to be active [31]. Also, employed is the self-consistent field (SCF) process at a meeting of 10^{-5} and Fermi smearing factor of 0.005 hartree to speed up its rate of convergence. The geometry optimization was gotten using the COMPASS force field and Smart minimization technique, a more geometrical optimization of the selected VR molecules was employed using neglect of diatomic differential overlap (NDDO) with AM1 Hamiltonian in the semi-empirical molecular orbital package VAMP (MS Studio 7.0) [32] Dynamic quantum chemical parameters like E_{HOMO}, E_{LUMO}, the energy gap ΔE (E_{LUMO}–E_{HOMO}), molecular surface area (MSA) and adsorption energy, respectively were acquired for the selected components of VR molecules to enable us ascertain their activity toward the Fe surface. All computations were thoroughly accomplished as controlled in the Materials Studio 7.0 software.

4 Results and Discussion

4.1 Weight Loss Method

The resultant outcome of the addition of VR at different concentrations on mild steel corrosion at 303 K was studied by a weight loss approach. This was tested within a period of 120 h immersion time. Figures 2a and 2b at 303 K revealed that the IE increased in the respective acid environment, and the corrosion rate decreased with an increase in the concentration of the inhibitor. The observed occurrence is associated with an increase in the adsorption of the inhibitor species resulting to the formation of a hydrophobic thin film on the acid/substrate interface. The inhibitor exhibited a maximum IE of 89.2 % and 98.4 % at a concentration of 1000 mg/L in 1 M HCl and 0.5 M H_2SO_4, respectively. The corrosion inhibition efficiency was obtained using the expression:

$$IE\% = \frac{(1 - W_{inh})}{W_{blk}} X\ 100 \quad (1)$$

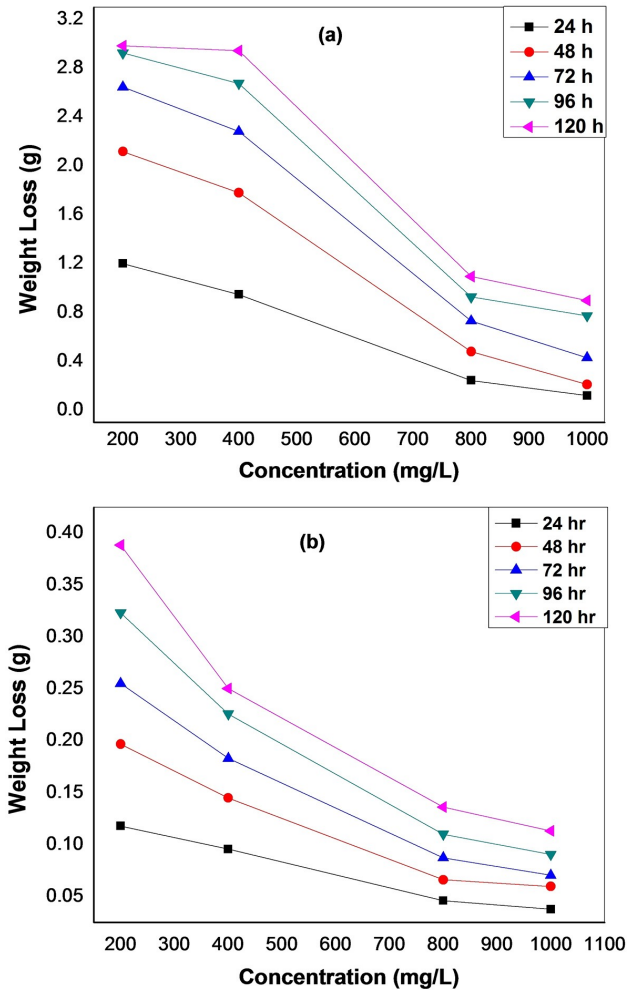

Fig. 2. Variation of weight loss with VR concentration for mild steel corrosion in: (a) 0.5 M H_2SO_4 and (b) 1 M HCl for different exposure time.

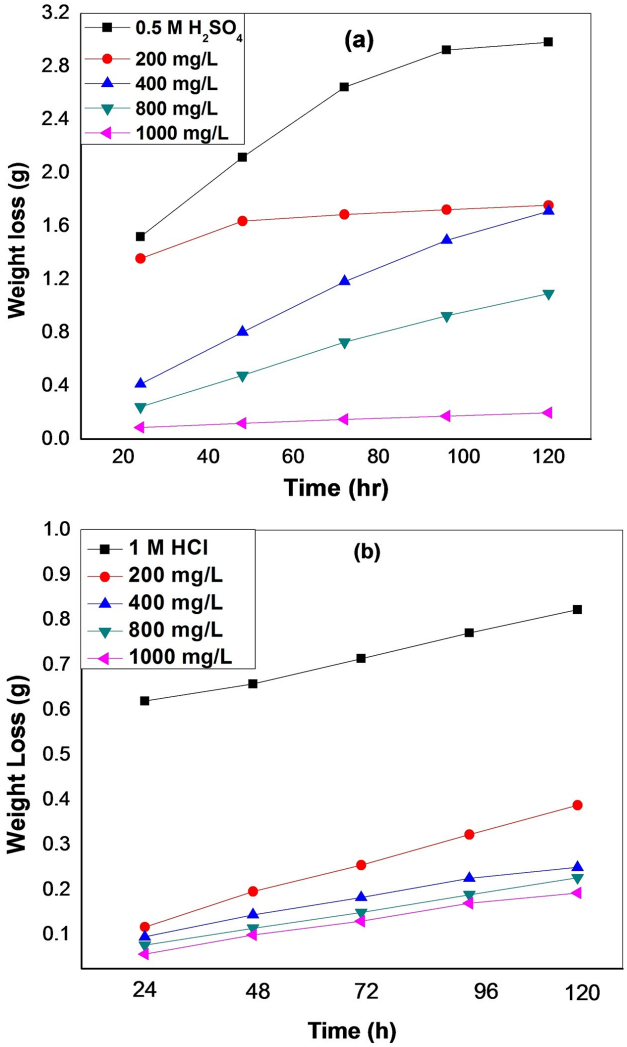

Fig. 3. Variation of weight loss with time for mild steel corrosion in: (a) 0.5 M H_2SO_4 and (b) 1 M HCl for different exposure time.

where W_{blk} and W_{inh} are the values of weight-loss of the steel after 120 h of dipping in solutions without and with the VR.

Figures 3a and 3b define the variation of weight loss and time. Careful scrutiny of the figure shows that weight loss increased with time, this could be due to desorption of the VR species adsorbed onto the surface of the metal over time.

4.2 Electrochemical Measurements

4.2.1 Open Circuit Potential Results

Figure 4a and 4b represents the open circuit potential results obtained in the absence and presence of VR extract in 0.5 M H_2SO_4 and 1 M HCl environments respectively. The results indicate that the solutions under investigation attained a considerable level of stable state before the commencing of the EIS and PDP experiment. The potential values tend to move towards the noble direction, showing a slight anodic effect on the corrosion inhibition process.

4.2.2 Potentiodynamic Polarization Results

The addition of different quantities of VR extract on the test solution exerted a pronounced effect on the electrochemical corrosion behavior of mild steel samples. Hence corrosion is electrochemical in nature (i.e cathodic and anodic half reactions), there is need to know the effect of VR on the different reaction types. Polarization studies provided flawless insight on the efficacy of VR on the half reactions. The PDP curves for mild steel in 0.5 M H_2SO_4 and 1 M HCl containing different concentrations of VR at 303 K are presented in Figure 5a and 5b. The useful extrapolated electrochemical parameters; corrosion potential (E_{corr}) and corrosion current densities (I_{corr}) acquired from the curves are listed in Table 1. The mild is seen to display fast dissolution. From the curves, no region of passivation was reported within the studied

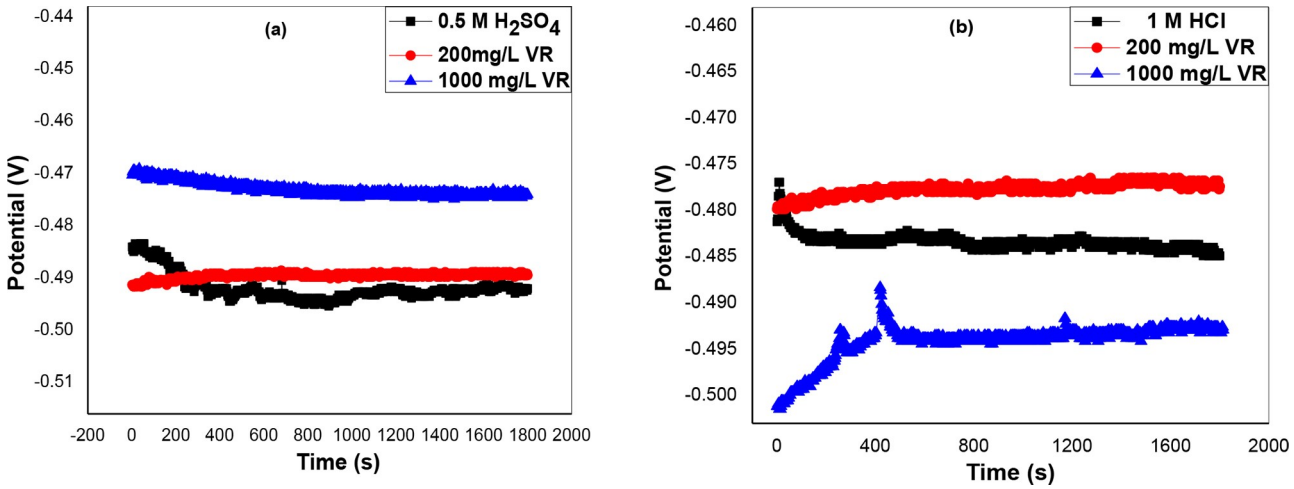

Fig. 4. Variation of potential with time in; (a) 0.5 M H_2SO_4 and (b) 1 M HCl showing the effect of VR extract.

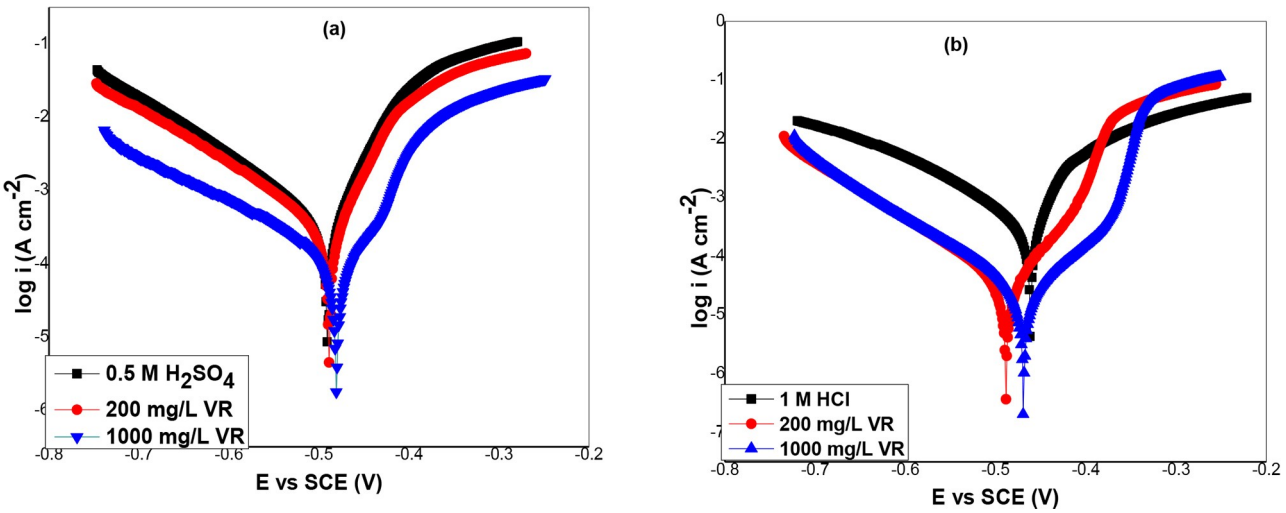

Fig. 5. Potentiodynamic polarization spectra of Mild steel in; (a) 0.5 M H_2SO_4 and (b) 1 M HCl showing the effect of VR extract.

Table 1. Polarization Parameters for Mild Steel in 0.5 M H_2SO_4 and 1 M HCl in the Absence and Presence of VR.

System	I_{corr} (μA/cm^2)	E_{corr} (mV vs SCE)	IE%
0.5 M H_2SO_4	173.8	−515.6	
200 mg/L VR	14.2	−507.4	91.8
1000 mg/L VR	5.9	−493.9	96.6
1 M HCl	193.5	−503.7	82.3
200 mg/L VR	34.2	−501.5	88.7
1000 mg/L VR	21.8	−534.2	

potential range. Polarization curves of the steel exposed in 0.5 M H_2SO_4 environment (Figure 5a) and 1 M HCl (Figure 5b) reveal that the incorporation of VR bends the cathodic and anodic curves towards lesser current densities. Considering previous reports, if the shift in E_{corr} is either above 85 mV or below 85 mV, the inhibitor can be described as cathodic or anodic type inhibitor, and if the displacement in E_{corr} is less than that the inhibitor can be seen as mixed type [4,9,12]. However, in this study, the displacement of E_{corr} was less than ±85 mV, which suggests a mixed-type inhibition mechanism, however, a slight shift of the corrosion potential towards the cathodic environment was observed in 1 M HCl environment.

From the given information in the Table 1, the I_{corr} retarded significantly upon the addition of VR compared to the uninhibited test solutions. The inhibition efficiency was calculated using the equation:

$$IE\% = \left(\frac{I_{blk} - I_{inh)}}{I_{blk)}}\right) x\ 100 \qquad (2)$$

where I_{blk} and I_{inh} represents the corrosion current density in the absence and presence of VR [33]. The highest inhibition IE value was recorded with the mild steel in 0.5 M H_2SO_4 inhibited system (96.6 %), followed by the

mild steel in 1 M HCl inhibited system (88.7 %) at VR concentration of 1000 mg/L at 303 K.

4.2.3 Impedance Spectroscopy Analysis

This technique was employed to have a clearer understanding of the electrochemical processes going on at the substrate/solution interface, and how they were affected by VR extract. Figures 6 and 7 reveal the impedance response of mild steel in the absence and presence of various concentrations of VR extract in 0.5 M H_2SO_4 and 1 M HCl environments. In the two impedance graphical representations, the plot for the uninhibited sample was employed as a reference for the inhibited sample at different concentrations. They plots presented in Figure 6a and Figure 7a are characterized by a single semicircle over the range of studied frequencies. It is important to state here that the high-frequency intercept with the real axis in the Nyquist plots is allocated to the solution resistance (R_s) and the low-frequency intercept with the real axis is ascribed to the charge transfer resistance (R_{ct}). The obtained impedance data were fitted with circuit models presented in Figure 8, using ZSimpWin 3.10 software. The circuit model shown comprises of a single CPE and charge transfer resistance elements which denote the impedance effect as a result of corrosion product species for the uninhibited environment. In this circuit, the CPE was used as a replacement for pure capacitance to recompense for the electrode surface unevenness frequently initiated by the buildup of corrosion products and lack of uniformity of the metal surfaces [29,30] including surface micro-defects.

The use of such CPE affords insight for the nonconformities from ideal dielectric behavior. The impedance, Z, of CPE is given as:

$$Z_{CPE} = Q^{-1}(g\omega)^{-n} \quad (3)$$

Here Q and n is the CPE constant and exponent, respectively, $g^2 = -1$ remains an imaginary number, and ω is the angular frequency in rad s^{-1} ($\omega = 2\pi f$ when f is the frequency in Hz), CPE can denote resistance ($Z_{CPE} = R$, $n = 0$), capacitance ($Z_{CPE} = C$, $n = 1$). The addition of different quantities of VR displayed an increase in the diameters of the convectional arc of the Nyquist plots, low frequency impedance magnitude ($|Z|$ 0.1 Hz) of the Bode modulus plots (see Figures 6b and 7b) and magnitude of the phase angle maxima of the Bode phase angle plots (see Figures 6c and 7c) these indicate corrosion inhibition. The increase is found to be concentration-dependent. Additionally, it was observed that the phase angle maxima were all significantly higher in the presence of the various concentrations of the VR when compared with the uninhibited system.

To estimate the obtained values of the corresponding impedance parameters shown in Table 2, the resultant spectra were evaluated with the aid of an equivalent circuit employed to model the metal/acid interface [6,29].

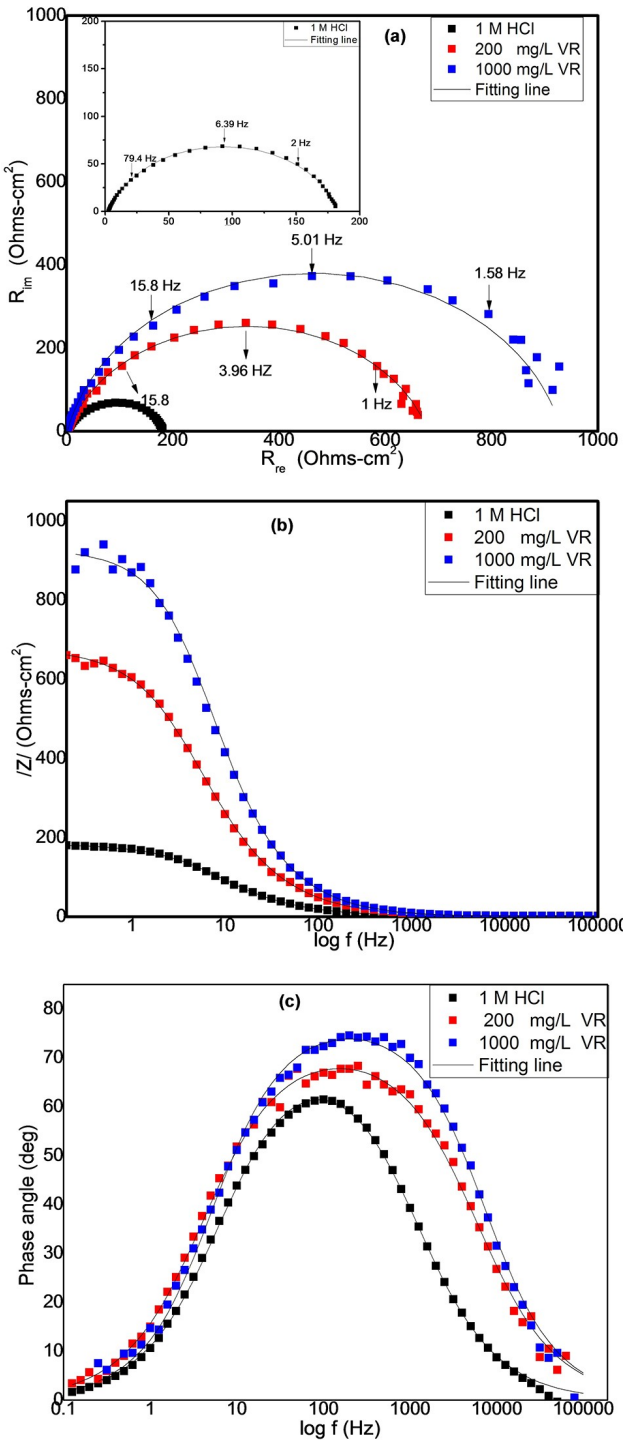

Fig. 6. Electrochemical impedance spectra of mild steel in 1 M HCl environment showing the effect of VR extract: (a) Nyquist plot, (b) Bode modulus and (c) Bode phase angle plot.

The diameter of the convectional arc of the impedance is associated to the charge transfer resistance (R_{ct}). The presence of VR extract in 1 M HCl (Figure 6a) and 0.5 M H_2SO_4 (Figure 7a) solutions resulted to a rise in the size of the Nyquist convectional arc in each case, this occurrence proved that inhibition actually took place.

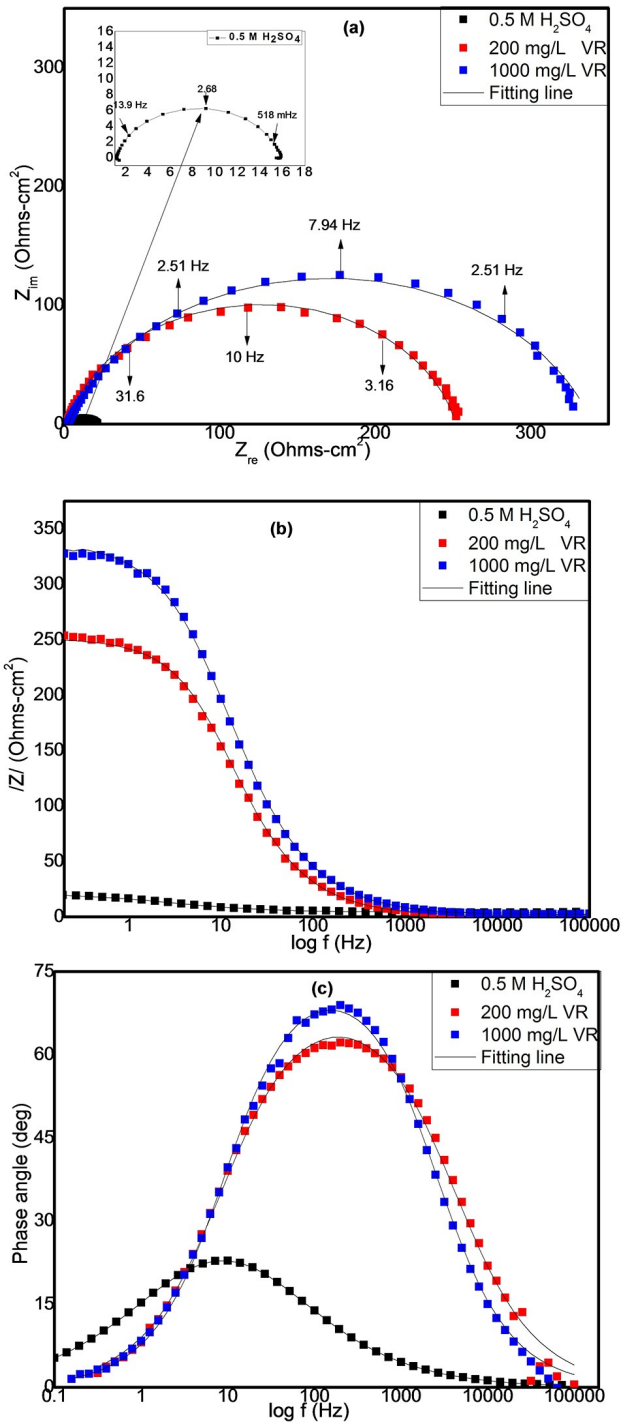

Fig. 7. Electrochemical impedance spectra of mild steel in 0.5 M H_2SO_4 environment showing the effect of VR extract: (a) Nyquist plot and (b) Bode modulus plot.

Careful scrutiny of the Nyquist plots show an increase in Rct values in the solutions containing VR, which manifested into the increase in the diameter of the Nyquist convectional arc and confirms the corrosion inhibiting influence of VR. The corresponding decrease in the CPE values in the presence of VR compared with the

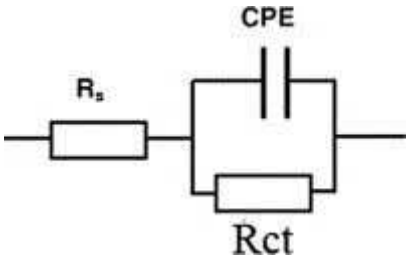

Fig. 8. Equivalent circuit diagram.

Table 2. Electrochemical Impedance Parameters for Mild Steel in 0.5 M H_2SO_4 and 1 M HCl in the Absence and Presence of VR.

System	Rs (Ωcm^2)	R_{ct} ($\Omega\ cm^2$)	CPE	n	IE%
0.5 M H_2SO_4	4.1 ± 1	15.2 ± 1.5	163 ± 0.4	0.78 ± 0.8	
200 mg/L VR	1.979 ± 0.8	249.8 ± 0.8	118.7	0.87 ± 0.3	93.9
1000 mg/L VR	2.436 ± 1.5	337.2 ± 1.5	120 ± 1.6	0.80 ± 0.6	95.5
1 M HCl	2.5 ± 0.7	181.2 ± 0.8	266.8 ± 1.3	0.82 ± 0.5	73.3
200 mg/L VR	1.8 ± 1.4	678.7 ± 1.3	105 ± 1.5	0.82 ± 0.4	80.5
1000 mg/L VR	1.681 ± 1.7	929.5 ± 1.3	50 ± 1.2	0.87 ± 0.4	

uninhibited system is an indication of the presence of organic species of VR at the metal/solution interface.

The IE% for various VR concentrations were calculated from impedance plots by means of the equation:

$$IE\% = \left(\frac{R_{ct(inh)} - R_{ct(blk)}}{R_{ct(inh)}}\right) x\ 100 \quad (4)$$

here $R_{ct(blk)}$ and $R_{ct\ (inh)}$ denotes the R_{ct} of VR when it has not been introduced and when it is present. Here again, the IE% values due to impedance follow the same trend with the Polarization data already discussed.

4.3 Adsorption Insights

The adsorption strength of organic inhibitors relies on many factors, among which are: the temperature of the reaction, the nature and charge on the substrate surface, the type of test environs and the conformation of the inhibitor [34,35].

Considering acid solutions such as HCl and H_2SO_4 a number of the organic components of the VR species exist in protonated form, whereas the remaining exists in non-protonated (molecular) state. The mode of adsorption would thus include the two factions, molecular species interacting with active sites on the steel surface, in addition to protonated species interacting with the pre-adsorbed chloride ions (from the corrodent) on the metal surface (in 1 M HCl environment).

The adsorption of the VR species was further described by fitting the surface coverage (θ) data obtained from gravimetric results to the Langmuir adsorption isotherm. Supposing the shielded parts of the steel surface are equivalent to zero, then corrosion is likely to have

taken place mainly on the exposed parts of the metal surface. The degree of coverage (θ) was calculated using the formula [36–39]:

$$\theta = 1 - \frac{w_{inh}}{w_{blk}} \quad (5)$$

here w_{blk} and w_{inh} represents, the weight loss values obtained in the absence and presence of VR. The adsorption isotherm relationship of Langmuir is explained by the equation;

$$\frac{C_{(inh)}}{\theta} = \frac{1}{K_{ads}} + C_{(inh)} \quad (6)$$

where $C_{inh,}\theta$ and K_{ads} signifies the inhibitor concentration, the extent of surface coverage and the stability constant for the adsorption-desorption process [40–45]. Figure 9 reveals the plots of $C_{(inh)}/\theta$ *vs* $C_{(inh)}$.

Accordingly, the plots obtained for VR are linear, with slopes of 1.0388 and 0.8543, in 1 M HCl and 0.5 M H_2SO_4 respectively. The correlation values ($R^2 = 0.9981$ and 0.9308) acquired at 303 K approve the validity of this method. The divergence of the slopes from unity can be associated with interactions between VR species on the metal surface and adjustments in the adsorption heat as the surface coverage increases [13].

4.4 Surface Analysis

4.4.1 SEM Scrutiny

This technique gives a pictorial illustration of the surface of the metal. The morphology acquired from the surface of the mild steel before and after immersion in the acid environs for a period of 24 h in the absence and presence of 1000 mg/L VR are shown in parts a, b, c, d and e in Figure 10, respectively. The SEM pictures of the substrate surface before immersion appears very smooth (Figure 10a), after immersion in the absence of VR (see in Figure 10b and 10c), results show that their surface is rough reflecting active dissolution in the acid environs. Additionally, without the inhibitor the surface of the metal sample in 0.5 M H_2SO_4 (Figure 10c) presented a coarse outlook in line with the weight loss results. Meanwhile, in the presence of VR (see Figure 10 d and e) the surface of the metal appears smoother compared with the uninhibited system (without VR). The result obtained at the highest inhibitor concentration is by reason of the presence of more VR species that were adsorbed on the mild steel surface, leading to better surface coverage.

4.4.2 AFM Scrutiny

The 3D AFM technique was used to carefully examine the look and the resulting impact of VR on the development of a corrosion reaction at the steel surface [26–28]. Figure 11 elucidates 3D AFM appearance of steel surfaces in the absence and presence of the best concentration of VR extract. Proper examination of the presented image in Figure 11a and b, indicates that the steel surface appears uneven by reason of rapid corrosive attack in the absence of VR. The average roughness of the metal surface submerged in 1 M HCl and 0.5 M H_2SO_4 were estimated to be 189 nm and 236 nm. Conversely, in the presence of the best concentration (1000 mg/L) of VR (Figure 11c and d) the coarseness was calculated to be 102 nm and 83 nm. The observed decrease in the extent of roughness is ascribed to the adsorption of a compact protective layer of VR on the substrate surface as explained earlier by impedance and SEM findings.

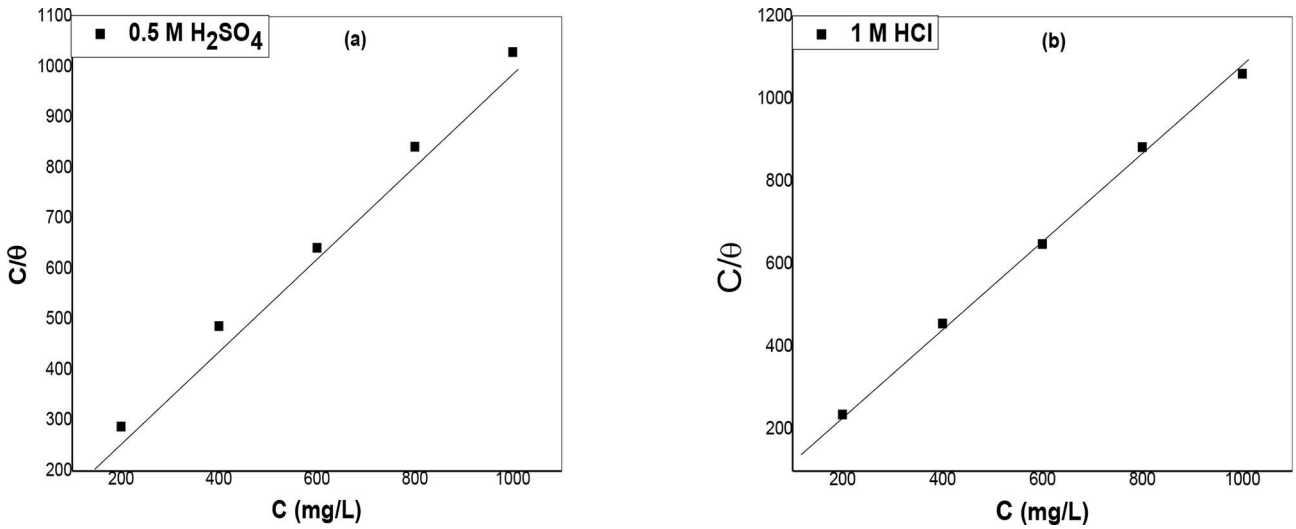

Fig. 9. Shows Langmuir adsorption isotherm for VR on mild steel in (a) 0.5 M H_2SO_4 and (b) 1 M HCl environment.

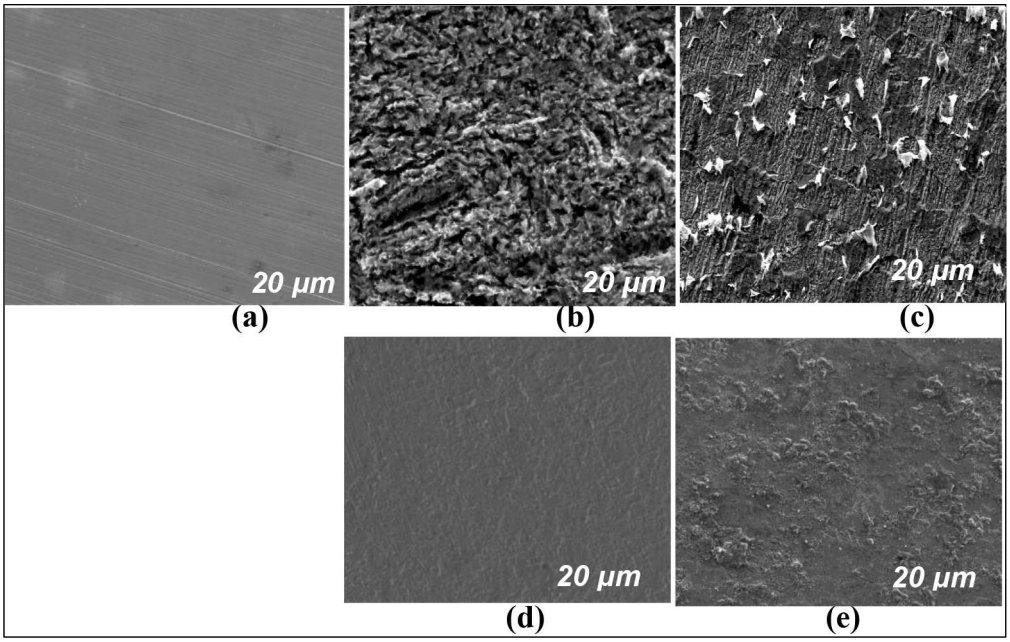

Fig. 10. SEM images of the mild steel surface after 24 h immersion at 303 K: (a) as received, (b) in 1 M HCl (c) in 0.5 M H_2SO_4, (d) in 1 M HCl + 1000 mg/L VR and (e) in 0.5 M H_2SO_4 + 1000 mg/L VR.

4.5 Computational Investigation

The application of computational chemistry in the motif and development of organic corrosion inhibitors has been significantly improved by the advances of density functional theory (DFT) and Molecular dynamic simulation (MD). In this period of software advancement, corrosion scientist can choose a good inhibitor on the ground of theoretical analysis of molecular properties of the corrosion inhibitor structures; this approach is both cheap and effective unlike the experimental approach. The use of the DFT and MD approach can correctly speculate the inhibiting tendencies behavior of inhibitor molecules utilizing molecular/electronic properties and reactivity hint/indices [46].

This approach is a very active field of research and many researchers have reported that inhibition effect mainly depends on some physico-chemical and electronic properties of the organic inhibitor which relate to its functional groups, electronic density of donor atoms, and orbital character of donating electrons etc.

It is therefore, necessary to carry out quantum chemical calculations in corrosion inhibition studies. Though there exist some peculiar challenges with this technique. For instance, till date, the identification of the components of the plant extracts that are responsible for the corrosion inhibiting performance still remain a major challenge. Interestingly, we have shown previously that DFT computations is worthwhile for theoretical assessment of the abilities of some extract components to interact with the Fe surface thereby affording insight on the species responsible the inhibition effect.

Herein, the DFT approach was adopted to provide in-depth explanation into the inhibitory mechanism of VR at the molecular level; vis-à-vis the adsorption properties of the

abundant species of VR on the Fe surface which are likely responsible for the corrosion inhibition action of VR. The selected species were the most abundant identified agents and includes: Caffeine (CF), 5-Hydroxylmethylfurfural (HMF), Linoleic acid (LA), and 3-O-Methyl-d-glucose (MG). Vital quantum chemical parameters such as $E_{LUMO,}$ E_{HOMO}, electrophilic, nucleophilic, the energy gap ΔE (E_{LUMO}–E_{HOMO}), absolute hardness (η), global softness ((σ) and adsorption energy were determined for the selected active constituents of VR were computed so as to provide their contribution towards the recorded VR inhibition performance. According to Koopman's theorem, the relationship between the energies of HOMO and LUMO orbitals and ionization potential and electron affinity of inhibitor molecule respectively is given in the expressions below [47–48].

$$I = -E_{HOMO} \tag{7}$$

$$A = -E_{LUMO} \tag{8}$$

Furthermore, the absolute hardness (η) and global softness (σ) of the inhibitor molecule are determined in terms of E_{HOMO} and $E_{LUMO:}$

$$\eta = \frac{I - A}{2} \tag{9}$$

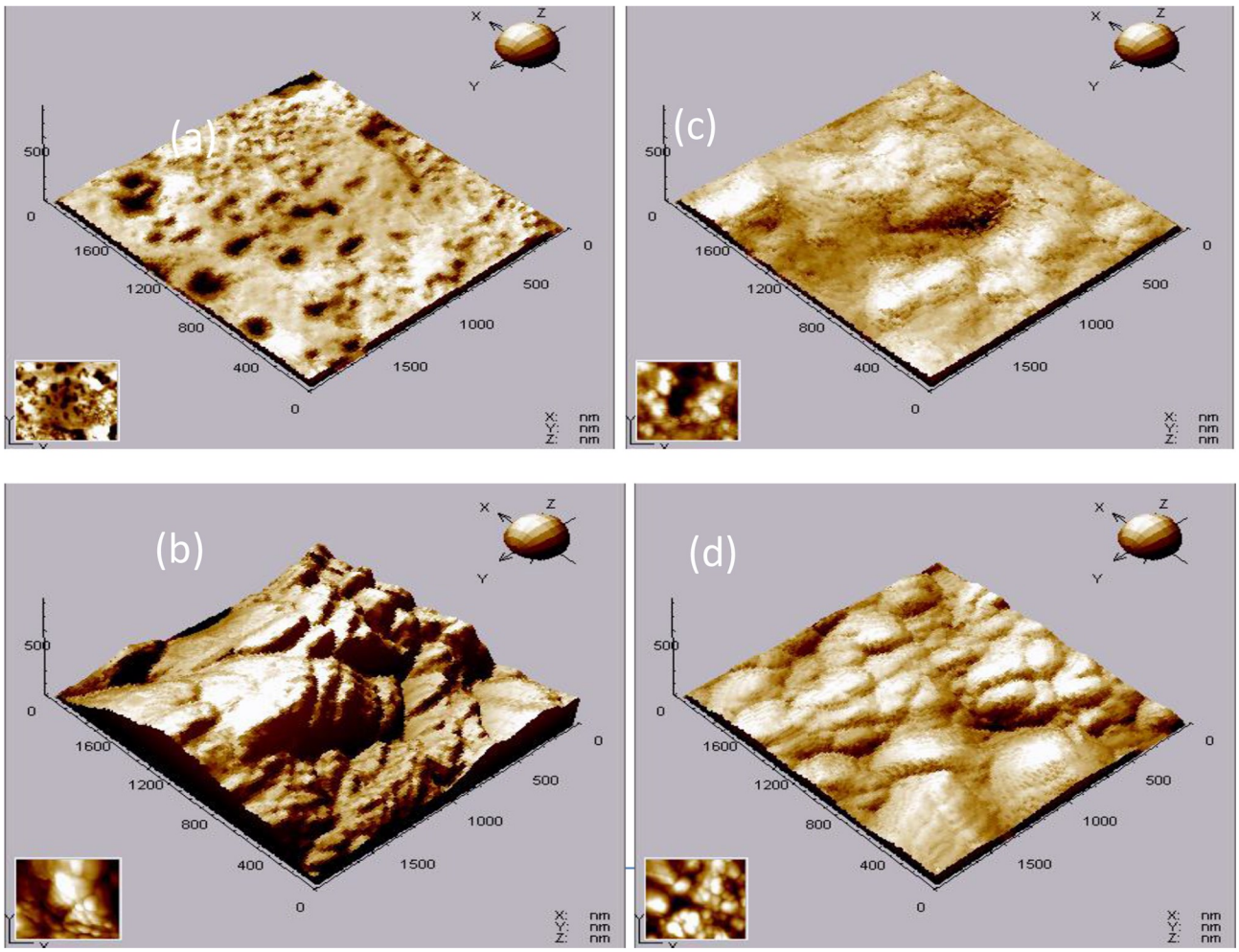

Fig. 11. AFM images of mild steel surface immersed for 24 h in: (a) 1 M HCl (b) 0.5 M H_2SO_4 (c) 1 M HCl + 1000 mg/L VR and (d) 0.5 M H_2SO_4 + 1000 mg/L VR.

$$\sigma = \frac{I}{\eta} \tag{10}$$

The parameters mentioned earlier were generated through geometric optimization with respect to all nuclear coordinates. Frontier molecular orbital theory is very suitable in envisaging the adsorption centers in the chosen VR constituents; these are responsible for interaction with the Fe surface. Figure 12 displays the optimized structure, the highest occupied molecular orbital (HOMO), the lowest unoccupied molecular orbital (LUMO) total electron density, electrophilic and nucleophilic of the active species of VR. The HOMO and LUMO energy orbitals are mostly saturated on the carbon/nitrogen atoms present in the chosen constituents. The Mulliken charges for the inhibitors indicate that the electronegative centers in the molecules are mostly concentrated in carbon, oxygen and nitrogen atoms. These atoms with enhanced electron cloud offer electrons to metal atoms during the adsorption process. The adsorption of the VR constituents on the Fe surface is as a result of the donor-acceptor interaction between inhibitor molecules and the Fe surface. The electron providing propensity of the chosen molecules is connected with the E_{HOMO}. It is important to note that a high value of E_{HOMO} means the propensity of inhibitor molecules to release electrons to the acceptor molecules having empty molecular orbitals. Furthermore, the tendency of a molecule to accept the electrons is associated to $E_{LUMO.}$ Lower values of E_{LUMO} reveal the easier reception of electrons from the Fe surface. The energy gap between the E_{LUMO} and E_{HOMO} energy levels, that is, ΔE of the molecule, is of significant consideration. Table 3 presents some quantum chemical parameters related to the molecular electronic structures of the most stable conformations of the selected VR molecules. From the results presented in Table 3 it is clear that all the obtained adsorption energies of selected molecules show a negative sign confirming a spontaneous adsorption process. From the data linoleic acid had the most negative value, followed by caffeine, 3-O-Methyl-d-glucose and finally 5-Hydroxy methylfurfural. The molecular surface area (MSA) values almost followed the same

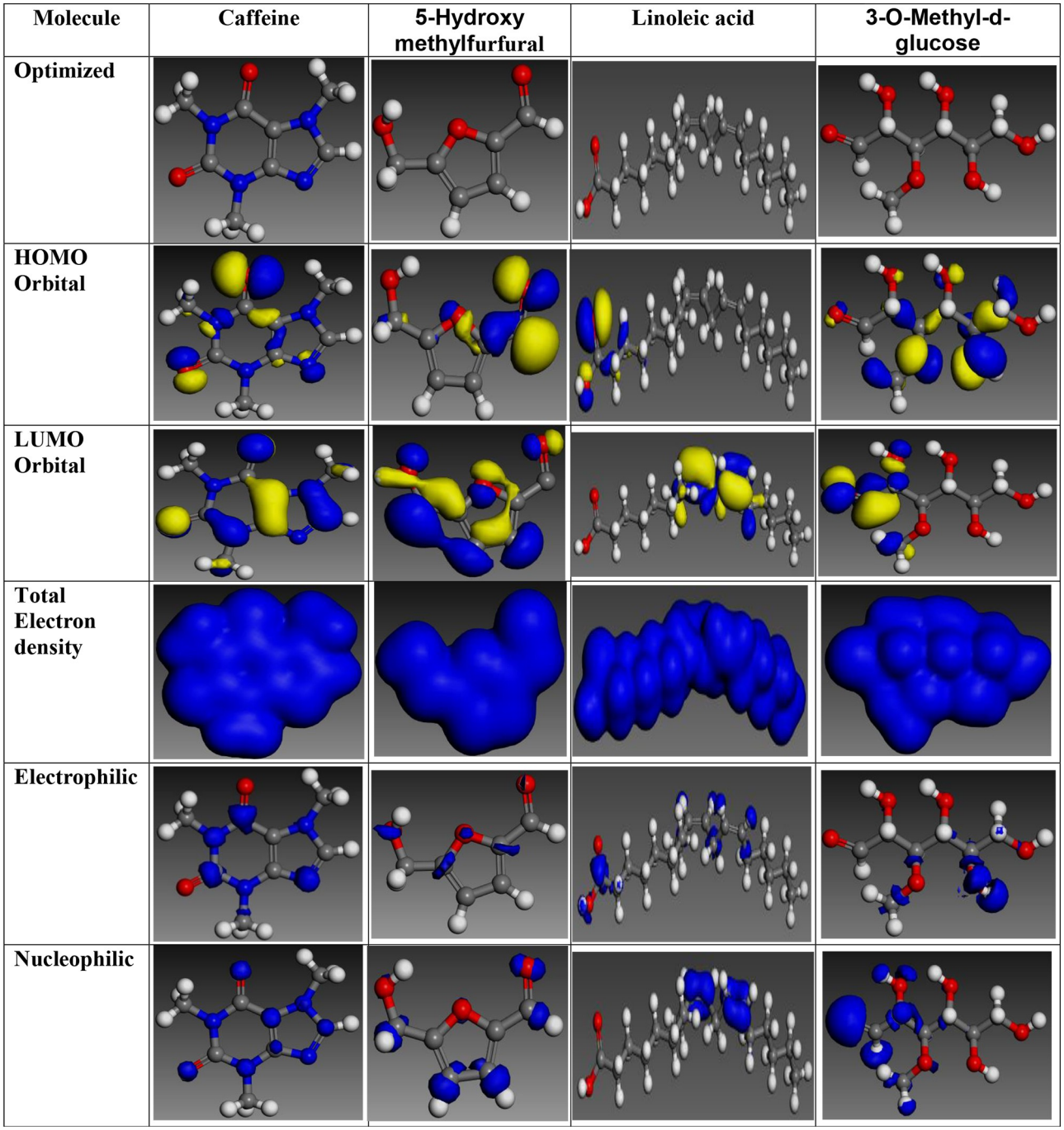

Fig. 12. Electronic properties of the selected constituents of VR, the blue and yellow isosurfaces depict the electron density difference: the blue regions show electron accumulation while the yellow regions show electron loss.

Table 3. Calculated Quantum Chemical Properties for the Most Stable Conformation of the Selected Constituents of VR.

Molecule	HOMO (eV)	LUMO (eV)	Energy Gap (ΔE)	Adsorption Energy (KJ/mol)	MSA (Å)	Global softness (σ)	Absolute hardness (η)
Caffeine	−7.096	−6.923	0.173	−134.2	228.8	11.6	0.0865
5-Hydroxy methylfurfural	−7.649	−7.548	0.101	−63.3	158.3	19.8	0.0505
Linoleic acid	−6.382	−6.159	0.223	−205.1	418.4	8.9	0.1115
3-O-Methyl-d-glucose	−5.988	−4.035	1.953	−115.5	230.8	1.02	0.9765

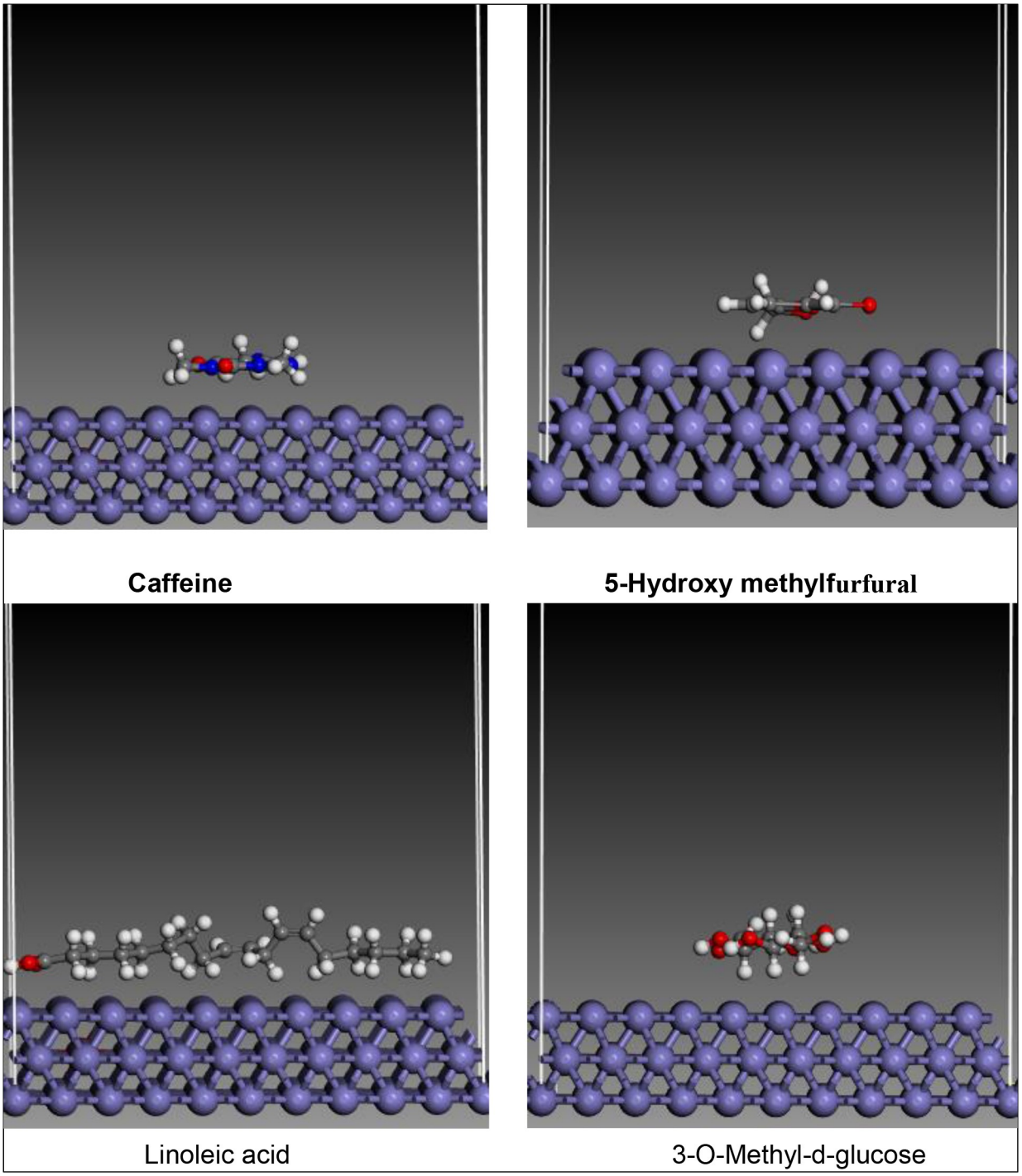

Fig. 13. Representative snapshots from molecular dynamics models of (a) Caffeine, (b) 5-Hydroxy methylfurfural, (c) Linoleic acid and (f) 3-O-Methyl-d-glucose; adsorption on Fe(110) Atom legend: white = H; gray = C; red = O; blue = N.

trend, with linoleic acid having the highest value followed by 3-O-Methyl-d-glucose, caffeine and 5-Hydroxy methylfurfural. Considering the HOMO, LUMO, electrophilic and nucleophilic sites present, it is obvious that there are possible sites through which these active components can donate and accept electrons in order to establish the observed bond between the inhibitor and the Fe surface.

Molecular dynamics (MD) simulation is simply a deterministic computational approach that has been popularly used by many researchers [48,49]. It simulates the natural pathway of molecular motion to sample successive configurations, following the classical Newtonian mechanics. This simulation was carried out in various ensembles, to sample different low energy adsorption configurations of the chosen extract constitu-

ents. This approach helps in determination of adsorption energies of some chosen VR extract constituents [4].

Four active constituents mentioned earlier were selected for computational modeling. Molecular dynamics simulations were employed to sample diverse low energy adsorption conformations of each molecule on the Fe surface [29,50]. The Fe slab for the simulations was cleaved along the (110) plane. The calculations were carefully carried out in a 10×8 supercell using a Compass force field and the Smart algorithm with NVE (micro-canonical) ensemble, a time step of 1 fs and simulation time of 5 ps. The Temperature was fixed at 350 K where we have a tradeoff. The system was quenched automatically at intervals of 250 steps. During simulation, the optimized structures of the four molecules (CF, HMF, LL, MG) and Fe (110) were used. The geometry of the bottom layers of the Fe (110) slab was well constrained, hence the energy of the forces that exist between them remained steady throughout the simulation time. This was not considered during the calculation; hence it will not affect the overall movement of the adsorbed molecule.

The lowest energy adsorption structures of the molecules on the Fe (110) surface are presented in Figure 13. Careful scrutiny of the snapshot revealed a flat/horizontal alignment onto the Fe (110) surface. This resultant alignment helped to increase the degree of surface coverage [47].

To properly measure the association between the molecules and the Fe surface under study, the adsorption energy (E_{ads}) of each system was calculated using the equation [46]:

$$E_{ads} = E_{total} - (E_{inh} + E_{Fe}). \quad (11)$$

Where E_{inh}, E_{Fe} and E_{total} represents the energy of the single molecule, the Fe slab without adsorption and the total energy of the system having the molecule and Fe surface, respectively. The data calculated by the software are shown in Table 3. The final adsorption energy was determined by averaging the energies of the five structures of lowest energy. The obtained values of the adsorption energy (E_{ads}) are presented in Table 3; the negative values of E_{ads} comply with a balanced/stable adsorption structure. Similar values of E_{ads} have been obtained elsewhere [50]. The calculated result via this technique shows that the selected individual components of VR extract effectively interact with the steel surface as corrosion inhibitors indicating that the recorded high IE % is due to the interaction of these and related active species of VR with Fe surface agreeing with the experimental results. Some researchers have demonstrated that there exists a good linear connection between IE and E_{ads}, in which IE, increased with an increase in the E_{ads} [3,34,50]. In view of the result presented in Table 3, the trend of E_{ads} (LL > CF > MG > HMF) shows that LL exerts a greater input to the overall impeding influence of VR extract.

5 Conclusions

The results demonstrated that VR extract inhibited the corrosion of mild steel in 1 M HCl and 0.5 M H_2SO_4 solutions. Significant IE values were observed in the investigated environs. It was observed that the IE, improved with extract concentration. PDP investigations show that the adsorbed VR species inhibited the corrosion development via a mixed-type mechanism, reducing both the noble dissolution of the substrate and the cathodic hydrogen evolution. The impedance results proved that VR inhibited the corrosion process through adsorption of its species on the metal/solution interface. The adsorption of VR was strongly validated by the Langmuir adsorption isotherm. SEM and AFM were used to study the surface morphology of mild steel. DFT established quantum chemical calculations of parameters linked with the electronic and adsorption structures of the four most abundant components of the VR extract substantiated their respective positive contributions to the observed inhibition efficacy of VR extract.

Acknowledgement

Support from the World Bank Africa Centres of Excellence for Impact (ACE Impact) Project (NUC/ES/507/1/304) is gratefully acknowledged. Demian I. Njoku acknowledges also, the National Natural Science Fund of China under contract No. 51871227 and No. 51650110506.

Data Availability Statement

The data that support the findings of this study are available from the corresponding author upon reasonable request

References

[1] I. Ali, N. Foaud, *J. Mate. Environ. Sci.* **2012**, *3*, 917–924.
[2] M. A. Amin, R. S. Bayoumy, S. S. A. El-Rehim, E. E. F. El-Sherbini, *Electrochim. Acta* **2007**, *52*, 3588.
[3] M. A. Chidiebere, E. E. Oguzie, L. Li, L. Ying, W. Fuhui, *J. Ind. Eng. Chem.* **2014**, *26*, 182–192.
[4] A. M. Abdel-Gaber, B. A. Abd-El-Nabey, A. M. El-Zayady, M. Saadawy, I. M. Sidahmed, *Corros. Sci.* **2006**, *48*, 2765–2779.
[5] H. Ashassi-Sorkhabi, M. Eshaghi, *J. Solid State Electrochem.* **2008**, *39*, 1497–1501.
[6] F. Bentiss, N. Chaibi, N. Lagrenee, B. Mernari, M. Traisnel, H. Vezin, *Corros. Sci.* **2002**, *44*, 2271–2289.
[7] M. Bouklah, A. El-Idrissi, B. Hammouti, A. Quassini, *Appl. Surf. Sci.* **2006**, *252*, 2178–2185.
[8] A. Bouyanzer, B. Hammouti, L. Majidi, *Mater. Lett.* **2006**, *60*, 2840–2843.
[9] M. A. Chidiebere, E. E. Oguzie, L. Liu, Y. Li, F. Wang, *Ind. Eng. Chem. Res.* **2014**, *53*, 7670–7679.
[10] L. R. Chauhan, G. Gunasekaran, *Corros. Sci.* **2007**, *49*, 1143–1161.
[11] L. R. Chauhan, G. Gunasekaran, *Corros. Sci.* **2004**, *49*, 4387–4395.

[12] M. A. Chidiebere, S. Nwanonenyi, N. Demian, N. B. Iroha, E. E. Oguzie, L. Ying, *World News of Nat. Sci.* **2017**, *15*, 1–19.
[13] E. E. Ebenso, E. E. Oguzie, *Mater. Lett.* **2005**, *59*, 2163–2166.
[14] G. Schmitti, K. Bedbur, *Werkst. Korros.* **1985**, *36*, 273–280.
[15] N. O. Eddy, S. A. Odemelam, I. N. Ama, *Green Chem. Lett. Rev.* **2010**, *3*, 163–172.
[16] R. Haldhar, D. Prasad, A. Saxena, A. Kaur, *Eur. Phys. J. Plus.* **2018**, *133*, 356 https://doi.org/10.1140/epjp/i2018-12165–0.
[17] A. Y. El-Etre, M. Abdallah, Z. E. El Tantawy, *Corros. Sci.* **2005**, *47*, 385–395.
[18] N. Patel, A. Rawat, S. Jauhari, G. Mehta, *Eur. J. Chem.* **2010**, *1*, 129.
[19] A. A. El-Hossary, R. H. Saleh, A. M. Shams El Din, *Corros. Sci.*, **1972**, *12*, 897–904
[20] U, R. Evans. The corrosion & oxidation of metals, Arnold Education, London. **1976**, *5*, 12–13.
[21] M. Gopiraman, V. Alexramani, D. Kesavan, S. Kim, I. P. Sakunthala, N. Sulachana, *J. Coat. Technol. Res.* **2012**, *9*, 15–26.
[22] E. E. Oguzie, *Mater. Chem. Phys.* **2008**, *99*, 441–446.
[23] E. E. Oguzie, *Corros. Sci.* **2007**, *49*, 1527–1539.
[24] C. A. Loto, O. O. Joseph, R. T. Loto, A. P. Popoola, *Int. J. Electrochem. Sci.* **2013**, *8*, 1187–11100.
[25] C. J. Lambrides, I. D. Godwin, K. Chittarajan, Genome Mapping & Molecular Breeding in Plants, **2006**, *3*, 69–90.
[26] K. K. Mogotsi, R. Wilczek, M. Brink, G. Belay, PROTA 1: Cereals & pulses/Céréales et légumes secs. PROTA, Wageningen, Netherlands, **2006**.
[27] I. U. Khan, S. Mahiya, B. S. Rathore, B. Singh, *Trends Biochem. Sci.* **2017**, *10*, 1588–1595.
[28] H. P. Hark, R. Corbett, B. Krantz, *NACC International, Houston, Texas.* **1998**, 98220.
[29] A. K. Ipadeola, N. Z. L. Mathebula, M. V. Pagliaro, H. A. Miller, F. Vizza, V. Davies, Q. J. F. Marken, K. I. Ozoemena, *ACS Appl. Mater. Interfaces* **2020**, *3*, 8786–8802.
[30] T. P. Mofokeng, A. K. Ipadeola, Z. N. Tetana, K. I. Ozoemena, *ACS Omega.* **2020**, *5*, 20461–20472.
[31] B. J. Delley, *Chem. Phys.* **1990**, *92*, 508–517.
[32] B. Gomez, N. V. Likhanova, M. A. Dominguez-Aguilar, R. Martinez-Palou, A. Vela, J. L. Gazquez, *J. Phys. Chem.* B **2006**, *110*, 8928–8934.
[33] M. J. S. Dewar, E. G. Zoebisch, E. F. Healy, *J. Am. Chem. Soc.* **1985**, *107*, 3902–3909.
[34] I. B. Obot, N. O. Obi-Egbedi, A. O. Eseola, *Ind. Eng. Chem. Res.* **2011**, *50*, 2098–2110.
[35] Fontana, M. G. (1986). Corrosion Engineering, McGraw-Hill Book Company, 282, 41.
[36] E. E. Oguzie, *Mater. Chem. Phys.* **2008**, *87*, 212–217.
[37] M. G. Hosseni, H. Khalilpur, S. Ershad, L. Saghatforoush, *J. Appl. Electrochem.* **2009**, *40*, 215–223.
[38] W. Hurlong, B. Rui, X. Jian, *Corros. Sci.* **2004**, *46*, 2455–2466.
[39] X. H. Li, G. N. Mu, *Appl. Surf. Sci.* **2005**, *252*, 1254–1265.
[40] G. Morelti, F. Guids, G. Gron, *Corros. Sci.* **2004**, *46*, 387–403.
[41] L. Mounium, B. Found, Michel, *Appl. Surf. Sci.* **2005**, *252*, 950–958.
[42] K. M. Nadkarani, (2001), Indian plants, Drugs, Asiatic Publish house New Delhi, 233.
[43] A. M. Popova, S. Christov, E. Raicheva, Sokolova, *Corros. Sci.* **2004**, *46*, 1333–1350.
[44] P. B. Raja, A. K. Qureshi, A. A. Rahim, H. Osman, K. Awang, *Corros. Sci.* **2013**, *69*, 292–301.
[45] P. B. Raja, M. G. Sethuraman, *Mater. Lett.*, **2008**, *62*, 2977–2979.
[46] S. A. M. Refaey, F. Taha, A. M. Abd El-Malak, *Appl. Surf. Sci.* **2004**, *236*, 175–185.
[47] Y. Hua, Y. Liu, J. Chen, *Eur. Phys. J. Plus.* **2018**, *133*, 524.
[48] M. J. Bahrami, S. M. A. Hosseini, P. Pilvar, *Corros. Sci.* **2010**, 52, 2793–2803.
[49] M. K. Awad, M. R. Mustafa, M. M. A. Elnga, *THEOCHEM.* **2010**, *959*, 66–74.
[50] C. J. Casewit, K. S. Colwell, A. K. Rappe, *J. Am. Chem. Soc.* **1992**, *114*, 10046–10053.

Received: July 29, 2020
Accepted: October 19, 2020
Published online on November 11, 2020

